NATIONAL ACADEMY OF SCIENCES

Number 41 • November 1960

IGY BULLETIN

A monthly survey of programs and findings of the International Geophysical Year and the International Geophysical Cooperation–1959 as related primarily to United States programs. The Bulletin also reports on international programs in geophysics and space science that have grown out of the IGY, and on their results.

Gravity Measurements on a Surface Ship at Sea

The following material is based on a more detailed report by J. L. Worzel, of the Lamont Geological Observatory, Columbia University. The earlier report appeared in the Journal of Geophysical Research, *September 1959.*

The restless nature of the sea has in the past made it extremely difficult to obtain measurements of the Earth's gravity over the 80% of its area covered by water, since such measurements must be made from a stable surface. Previously, it was possible to make only a relatively small number of oceanic observations from submarines resting at quite depths. However, with the development a few years ago, by Anton Graf of Munich, Germany, of a new submarine gravimeter that J. L. Worzel was able to adapt for use on a stabilized platform aboard a surface ship, gravity measurements can now be made successfully at sea anywhere in the world.

A detailed description of the instrument, operational procedures, and computation and correction methods is given in the *JGR* report mentioned above, and an account of the first marine test of the Graf Sea Gravimeter appears in *Bulletin No. 8.* The present report reviews the results of further sea-surface experiments made aboard the *USS Compass Island,* an 18,000-ton US Navy vessel fitted with a stabilized platform. The cruise, conducted during a five-week period in March and April 1958, covered portions of the North Atlantic and Mediterranean Sea (see Fig. 1).

Captain L. L. Schock of the Navy's Bureau of Ordnance made arrangements for the test series, and the officers and crew

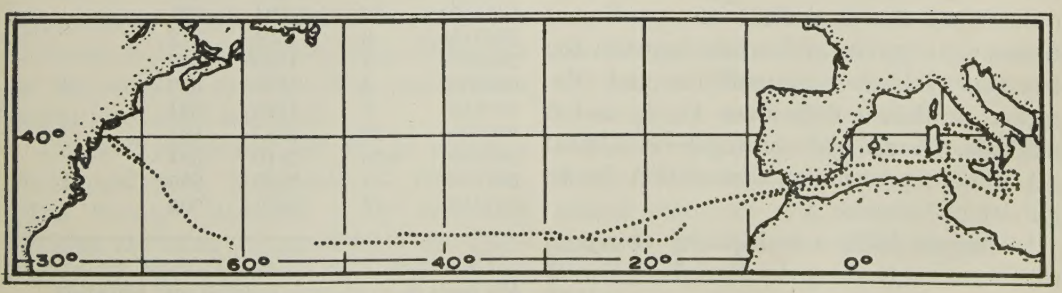

Fig. 1. *Portions of the Cruise Track of* USS Compass Island *in the Atlantic Ocean and Mediterranean Sea, in March–April 1958, Along Which Gravity Measurements Were Made.*

of the *Compass Island*, under the command of Captain J. A. Dare, gave very important assistance. V. R. Sinclair, J. G. Gallagher, and G. Pritchard participated in the observation program, which was directed by J. L. Worzel, and Annette E. Trefzer assisted with computations and drafting of figures. Important advice and encouragement were received from Maurice Ewing and Merle Tuve. The project was sponsored by the US National Committee for the IGY, of the National Academy of Sciences, and supported by a National Science Foundation grant.

Cruise Measurements

Calibration measurements based on comparisons with measurements made by a Frost gravimeter show that the Graf Sea Gravimeter measures gravity satisfactorily on land; that the meter also makes satisfactory measurements on a submerged submarine was shown by Worzel and Graf in 1957; and comparisons with previous observations made at various base stations (the New York Naval Shipyard, the Naples area, Italy, and at two locations in the harbor at Palma, Majorca, in the Western Mediterranean) show that the meter gives satisfactory results on a surface ship in harbors. The observations reviewed in the present report demonstrate that gravity measurements can now be made successfully on a surface ship at sea.

One of the early cruises of the *Compass Island* crossed three profiles of gravity data previously made with Vening Meinesz pendulums off the east coast of the United States. The gravity differences between the *Compass Island* measurements and the earlier pendulum data were 11, 6, and 6 milligals. (A milligal—or mgal—is 1/1000 gal, which represents an acceleration due to gravity of 1 cm/sec^2.)

In August 1958, a multiplicity of repeat runs were made along the New York line of submarine gravity observations of the *USS Tusk* in 1947 and duplicated in 1957 by the *Compass Island* in the first oceanic test of the Graf gravimeter (see *Bulletin No. 8*). One of these runs was the only one on which it was possible to make simultaneous observations with two instruments mounted on the same stable platform.

The maximum spread of the observations for the different runs with one meter is 20 mgal. The difference between the two meters recording simultaneously on a single run was essentially zero. The 20 mgal spread must, therefore, be attributed to the fact that the runs were not made over identical courses and to a lack of precise knowledge of the speed over the "ground," needed for computing the Eötvös correction (correction applied to observed gravity values to account for the effects of changes in the ship's centrifugal acceleration owing to the rotation of the Earth; these changes depend primarily on the east-west component of the ship's motion). The agreement with

Table 1—Comparison of Gravity Observations at Crossings of the Ship's Own Track

Date and Time	Anomaly* (mgal)	Depth (meters)	Course (degrees)	Approximate Difference** (mgal)
250515	−17	2006	091	
300815	−21	2001	312	4
300830	−17	1869	312	
291145	34	572	181	
291200	37	572	183	
040745	28	539	091	11
040800	24	587	091	
292115	20	732	001	
040630	23	662	091	0
040645	12	977	091	
300600	18	1158	196	
300615	21	839	196	0
040545	22	894	091	
300715	6	1324	312	
300730	−4	1516	312	
040500	4	1350	093	3
040515	9	1723	091	
060930	−29	2359	091	
060945	−18	2110	091	
061730	−8	2332	295	1
061745	−17	2109	295	

* Variation from theoretical value expected on the basis of geographic location and elevation.

** "Approximate" because of navigational uncertainties.

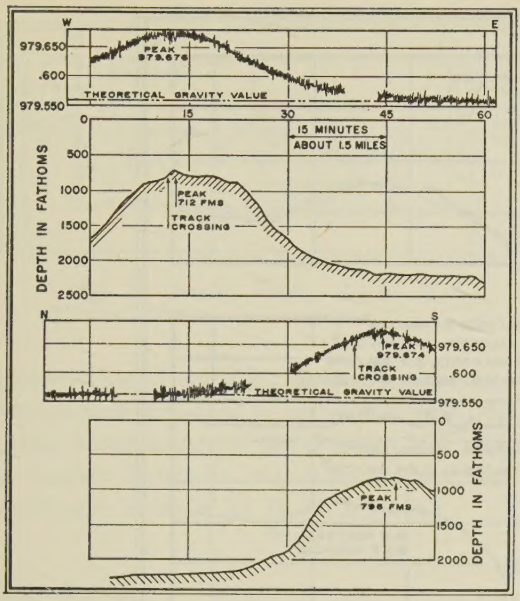

Fig. 2. *Gravity Profiles and Bottom Topography Along N-S and E-W Crossings of a Seamount Just North of Bermuda.*

previously made pendulum observations is as good as could be expected if the navigational errors of the two sets of observations and the differences of positions are considered.

Table 1 shows gravity variations for six crossings by the *Compass Island* of its own track in the Mediterranean when cruising on different courses. The navigation along these tracks was by celestial observations, radar fixes on shore as opportunity permitted, and dead reckoning. The approximate gravity differences were obtained by interpolation to the indicated crossing point between the values computed regularly at 15-minute intervals. These differences are referred to as approximate because of the uncertainties inherent in the navigation. The differences for the crossings are thus even smaller than might have been expected.

Figure 2 represents two tracks across a submerged peak just north of Bermuda. (The "free-air" anomaly is the difference between the observed gravity and the theoretical gravity given by the International Formula of Gravity.) Two crossings were also made of Caryn Peak, a much smaller feature beyond the mouth of the Hudson Submarine Canyon, which cuts the sea bottom on the continental shelf for more than 200 miles southeastward from the mouth of the Hudson River. The gravity signature is much smaller than for the peak north of Bermuda but it is still quite definite.

A west-to-east track across Cruiser Seamount, several hundred miles south of the Azores, is represented in Figure 3. The figure also shows seismic refraction measurements made on the seamount as well as seismic observations made on a previous cruise in locations similar to the flanks of the seamount but about 100 miles to the north. These gravity and seismic data, along with seismic-velocity and rock-density information compiled by J. E. Nafe and C. L. Drake, have permitted M. Talwani, of Lamont, to compute the shape of the Mohorovičić discontinuity (interface between the Earth's crust and the denser mantle directly beneath it) in the vicinity of the Cruiser Seamount. Although Talwani represented the seamount as a two-dimensional structure in these calculations, only minor changes would be required (probably less than a two-kilometer change in position of the M-discontinuity) in recomputations on the basis of a three-dimensional structure. Nevertheless, this diagram is substantially correct. It is interesting to note that it took only one day to observe and compute the gravity and two days to plot and compute the section.

Two crossings of the Tyrrhenian Sea were also profiled, and previously observed submarine gravity points within five miles of the *Compass Island's* track were plotted for comparison. The agreement between the two tracks is generally satisfactory.

Figure 4 shows a section across the Canary Basin. To the right, the track crossed an unnamed seamount and Ampere Bank. One previous pendulum observation made by Vening Meinesz, near the center of the section, shows excellent agreement. It is obvious that such a profile provides a much

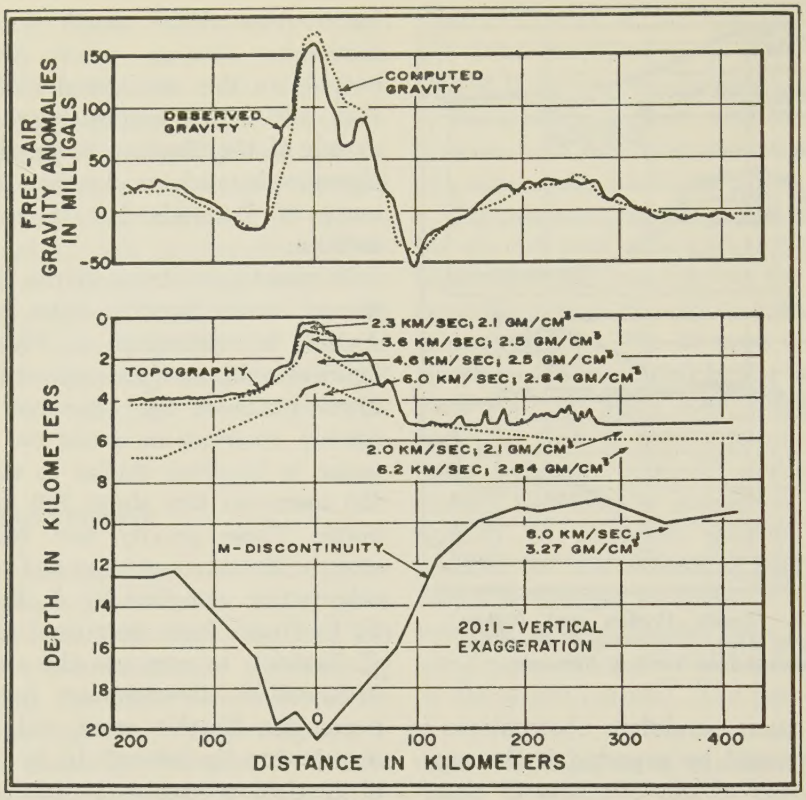

Fig. 3. *Gravity Profile of W-E Crossing of Cruiser Seamount, South of the Azores. Bottom Topography, seismic velocities in the crust and mantle, and configuration of Mohorovičić Discontinuity shown in lower portion of chart.*

better basis for picking a representative value of gravity for an area than is provided by observations at specific points. The roughness of the gravity curve indicates that topography similar to that of the Mid-Atlantic Ridge to the west and of the Continental Rise to the east must be buried beneath the Madeira Abyssal Plain.

A section across the Mid-Atlantic Ridge is shown in Figure 5. Again, it is obvious that a much more representative gravity

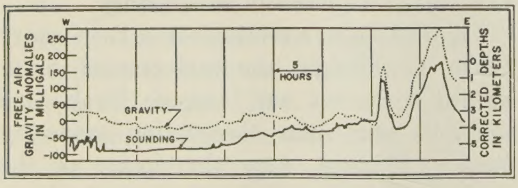

Fig. 4. *Canary Basin Gravity Profile. Unnamed seamount and Ampere Bank at right.*

anomaly value for an area can be determined from such a continuous curve than from individual points.

Figure 6 shows the results of two passages, never less than five miles apart, through the Strait of Gibraltar. The most obvious feature is the double negative anomaly, of the order of 100 mgal, shown by arrows on the chart. The agreement between the two passages is very impressive.

Since the cruise tracks were separated by at least five miles, it is obvious that the trend of the negative anomalies is almost north-south. It is important to point out that the existence of this double negative would probably never have become known from submarine gravity measurements because ship traffic is so dense in this region that it is almost impossible to make a submerged run of sufficient duration without

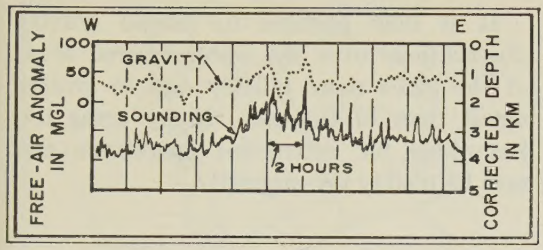

Fig. 5. *Gravity Profile Across Mid-Atlantic Ridge.*

serious risk of collision. It is probable that the eastern negative is associated with the Atlas Mountains and the western one with a former Paleozoic mountain system, according to a study by H. D. Klemme.

Conclusions

On a five-week cruise to the Mediterranean Sea aboard the *USS Compass Island* in March and April of 1958, it was possible to make gravity measurements 70% of the time. Observations were made 50% of the time in the Mediterranean. Since the limiting factor was the vessel's vertical heave, this record could have been greatly improved if the ship's course had been chosen for the benefit of gravity observations. Vertical heave is minimized when heading into the swells and maximized when heading across the swells.

The observations described above indicate that continuous gravity measurements can be made at sea with a precision of ±5 mgal using the Graf Sea Gravimeter mounted on a stable platform on a surface vessel. Some uncertainties arise, principally from the Eötvös effect and from the difficulty of determining the ship's precise location. When it becomes possible to determine a ship's position and speed over the bottom more accurately, the precision of the measurements should improve considerably.

The continuous curves produced by this technique greatly enhance the value of gravity observations at sea. They permit more representative gravity values, as are required for many geodetic studies, to be chosen for ocean areas. The interpretation of gravity anomalies depends almost entirely on the shape of the observed curve. Thus, a continuous curve is obviously much better for this purpose than a curve drawn to fit a number of discrete points. Continuous curves reduce the chance of errors in calculation that are always present in computations based on discrete observations. Continuous observations also prevent the overlooking of new features whose existence was not anticipated.

It remains to be seen whether the Graf Sea Gravimeter can be used successfully on smaller, unstabilized vessels. A stable platform and a Graf Sea Gravimeter have been installed on the Lamont Geological Observatory's 500-ton, 200-foot research vessel *Vema*. It was expected that observations from such a vessel could be made for a smaller fraction of time, however, because a small vessel would be more readily

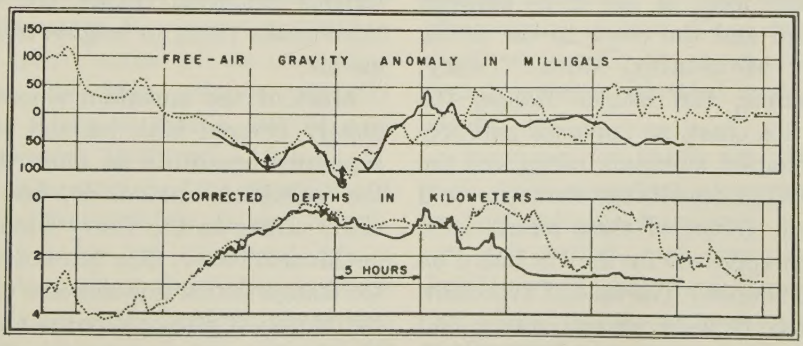

Fig. 6. *Two Gravity Profiles Through Strait of Gibraltar. Arrows indicate minima in the gravity anomaly waves.*

and more completely affected by swells than would a larger vessel. (Since publication of the September 1959 *JGR* report on which the present material is based, Lamont investigators aboard the *Vema* have completed a 560-mile gravity profile.)

It is now possible to extend gravity observations over the water-covered areas of the globe more quickly and in greater detail than in the past. Many areas too hazardous for submarine operations can now be readily investigated.

Geological Observations in West Antarctica During Recent Oversnow Traverses

The following material is based on a report by George A. Doumani of the Institute of Polar Studies, Ohio State University. Mr. Doumani participated in seismologic and glaciologic studies at Byrd Station, and was a member of the two oversnow traverses discussed below, during 1959 and early 1960.

General geological investigations were conducted at accessible rock exposures in Marie Byrd Land west and north of Byrd Station during two major oversnow traverses in 1959 and 1960. The first, an IGC-59 traverse to the Executive Committee Range, was made in the austral autumn of 1959. The observations were made mainly at Mount Sidley, highest and most prominent feature of the Executive Committee Range. (See Figure 7.)

The following spring, a reconnaissance flight covered most of the areas between Byrd Station and the coast to the north. The Crary Mountains, Mount Toney, Mount Takahe, the Kohler Range, the Amundsen Sea coast, an unnamed and previously uncharted mountain range, and the Executive Committee Range were inspected from the air. (Some of these names have not yet been approved by the US Board on Geographic Names.) The second over-snow party, in the 1959–60 austral spring and summer, followed a similar route. Rock specimens were collected from most of these areas, from Mount Petras, and from the Clark Mountains of the Edsel Ford Ranges.

This report summarizes the geological information gathered on these expeditions. More detailed reports on specific areas are in preparation. Major geologic and geographic features of the regions visited are outlined in Table 2.

Coordination and administration of the United States Antarctic Research Program since the termination of the IGY has been the responsibility of the National Research Foundation. See *Bulletin No. 39* for information on the status of the over-all Antarctic Program.

General Physiographic Description

The mountains in the western part of Marie Byrd Land exhibit certain physiographic consistencies. They are not continuous mountain chains, but rather isolated peaks rising to heights of about 4200 meters.

Most of the mountain slopes are completely covered with ice and snow. Rock exposures constitute no more than 5% of the individual mountains, and are especially scarce in the Crary Mountains and on Mount Toney. The Executive Committee Range shares this scarcity of exposures but morainal glacial deposits are abundant on the ice surface where valley glaciers merge to form piedmont glaciers. In the northern coastal ranges, on the other hand

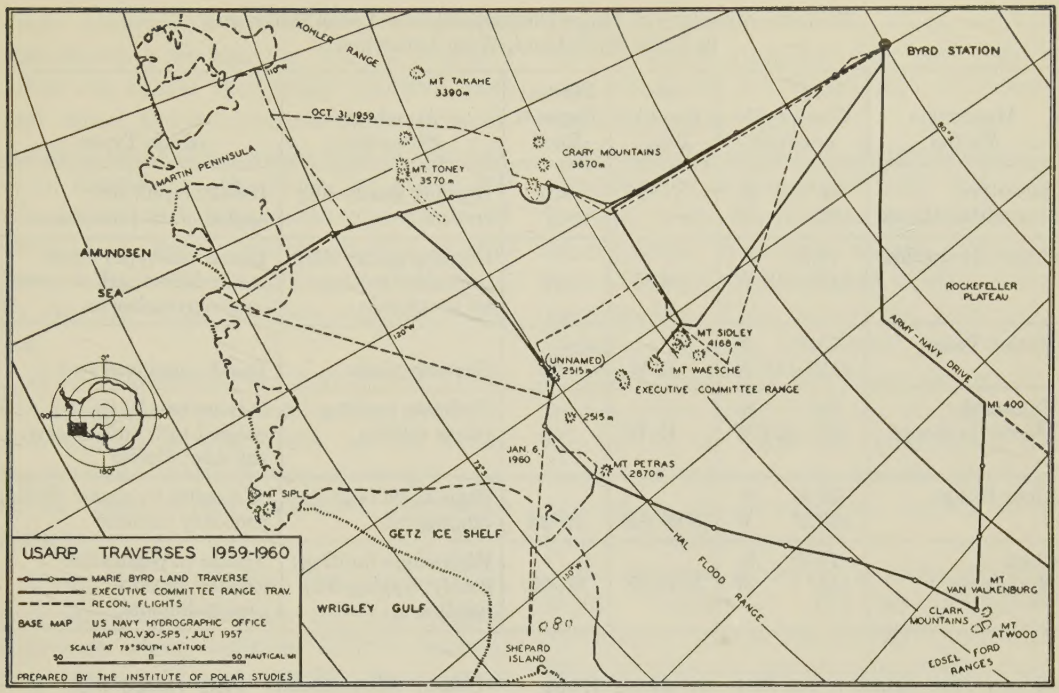

Fig. 7. *Traverse Routes in Region North of Byrd Station, Antarctica. Elevations in meters above sea level.*

—the Hal Flood and Edsel Ford ranges, and Mount Petras—whole mountains are commonly well exposed, and geological investigation is relatively easy.

Geologic Summaries for Regions Visited

Executive Committee Range: Four major mountains form the Executive Committee Range. Although these mountains are apparently connected with each other above sea level, ice covers the connecting areas as well as a great portion of the mountains themselves. The range trends generally north-south along longitude 126°W and between latitudes 76.5° and 77.2°S.

Most prominent of the four mountains of the range is Mount Sidley, an extinct volcano whose crater has developed into a cirque—a steep-sided, bowl-shaped recess commonly found at the head of a mountain glacier. The cirque walls rise about 1500 meters to the highest peak, which reaches an elevation of 4200 meters. The volcanic nature of Mount Sidley also characterizes the remainder of the range.

The south-eastern slope of the Executive Committee Range exhibits a conspicuous stratigraphic sequence of five tentatively-classified rock units. The lowermost unit is olivine basalt—a dark, extrusive igneous rock rich in the iron-magnesium silicate, olivine. At an elevation of about 2000 meters, the basalt surface displays sharp, symmetrical grooves, 10–15 centimeters in depth, apparently the result of abrasion by rock fragments imbedded in slowly flowing glacier ice.

Overlying the basalt are three distinct rock units consisting of compacted, fine-grained volcanic fragments, or tuff. They are red, yellow, and gray, in ascending order, and the lowest of the sequence lies unconformably upon the basalt. (An "unconformity" is a break in the depositional sequence of the rock strata in which younger

Table 2—Summary of Major Characteristics of Some Mountains in Marie Byrd Land, West Antarctica

Mountains Visited	Geographic Location	Geographic Trend	Percent Exposed Rock	Apparent Structure	Rock Types
Executive Committee Range	76°–77° S 126° W	N–S	<5	Dipping gently SE; craters	Basalt; lapilli tuff; agglomerates; moraines
Crary Mountains	76.9° S 116°–118°W	E–W	<5	Dipping gently SE; probable faulting on north side	Basalt (aa-type) flows; mafic dikes; agglomerates; coarse pyroclastics
Mount Toney	75.7° S 115°–116°W	E–W	<5	Craters; plugs	Basalt; agglomerates
Unnamed Mountain Range	76° S 123°–125°W	E–W	<5	Probable faulting; minor folding	Olivine basalt; light-colored tuff; tuff-breccia; rhyolite; diorite
Ames Range	75.8° S 128.2° W	NW–SE	20–25	High-angle faulting; dipping SE	Aphanitic to coarse felsite, probably rhyolite
Clark Mountains	77.3° S 142° W	NW–SE	90–95	High-angle faulting; gently dipping SE; jointing	Aplitic to pegmatitic granite; diorite; metasediments

strata rest upon a surface resulting from earlier erosion of the underlying older rocks.) These units are characterized by strong fragmentation and an abundance of accretionary lapilli—volcanic pellets, commonly with concentric structure. Cross-bedding, intercalation of strata, and partial rounding of the volcanic fragments characterize the gray tuff, which thus resembles a river deposit.

Glacial moraines are the uppermost deposits in the Mount Sidley rock sequence. Huge boulders of varying composition lie in a spectacular array of concentric arcuate patterns indicating stages of recession of the glacier ice. Large, well-developed crystals of anorthoclase feldspar found embedded in a boulder of reddish, vesicular lava are being used at present for age determinations by the potassium-argon radioisotope technique. Numerous boulders are strewn as far as 25 kilometers south of Mount Sidley, forming no apparent pattern. Their presence at such distances and their mode of occurrence raise questions concerning the mechanism by which they were carried to their present locations and deposited.

Crary Mountains: This range also consists of four main mountains; three have very prominent peaks, the highest attaining an elevation of more than 3700 meters. The mountains extend roughly east-west along 76.9°S and between 116° and 118°W.

The south side of the range slopes gently southward, meeting the ice cap in a relatively smooth incline. Ice covers more than 95% of the slopes of the range, but the few accessible outcrops permitted some geological investigation. The dominant rock type is a dark, extremely fine-grained basaltic lava containing larger almond-shaped crystals of feldspar similar to the anorthoclase from Mount Sidley (above). Highly contorted lava "bombs," evidence of explosive eruptive activity, occur both where they fell and as glacier-transported "erratics."

The north side of the range is steeper than the south side, and the ice cascading down the northern slopes is heavily crevassed. A well-exposed bedrock outcrop exhibits a succession of highly weathered lava flows, with characteristic caterpillar configuration. Clinkers similar to Hawaiian aa-type lava (rough, jagged, spiny basaltic lava) are clearly displayed. Two small

mafic (composed primarily of magnesian rock-forming silicates, or "dark minerals") dikes cut across the gently inclined flows and trend toward the mountain summit. Another mafic dike, to the west of this outcrop, extends up the slope for about 300 meters. All of these dikes appear to be vertical. A deep, vertical groove on the face of the northern outcrop, probably cut by running water, suggests seasonal thawing.

Mafic volcanic rocks—porphyritic olivine basalts, agglomerates, and coarse pyroclastics—appear characteristic of the entire range. Hand specimens are strikingly similar to those of the Executive Committee Range.

Mount Toney: Mount Toney is an elongate topographic feature trending roughly east-west along latitude 75.7°S between longitudes 115° and 116°W. The highest peak, apparently on the rim of an ancient volcanic crater, attains an elevation of approximately 3700 meters. The altitude of the main ridge decreases gradually from east to west and, as in the Crary Mountains, the southern slopes are gentle while the northern slopes are precipitous. Seismic soundings on the traverse showed that the bedrock surface beneath the ice between the Crary Mountains and Mount Toney is below sea level.

The only bedrock exposures on Mount Toney are on the northern slopes and constitute not more than 1% of the surface area. Examination of these exposures suggests that volcanics and agglomerates probably make up the major portion of the mountain. A mafic outcrop (of lamprophyric composition) occurs on the northeastern side of Mount Toney. This outcrop resembles a volcanic plug—solidified material filling the vent or pipe of a dead volcano. A circular, crater-like outcrop was seen from the air near the northeastern edge of the mountain.

Unnamed Mountain Range: This range consists of two major mountains and a low ridge, extending east-west along latitude 76°S between longitude 123° and 125°W and about 50 kilometers east of Mount Petras (see Fig. 7).

The eastern mountain is predominantly composed of light-colored tuffs and tuff-breccias, with conspicuous lamination and stratification. Brownish basalt crops out east of the tuff and probably overlies it unconformably. This basalt has been subjected to intense mechanical weathering, resulting in stepped, tombstone-shaped pinnacles, which occur from the ice surface to the top of the mountain. Underlying the basalt is a thin layer of rhyolite (the fine-grained to microcrystalline equivalent of granite) containing pyrite.

The western mountain is composed of a diorite "basement" rock unconformably overlain by olivine basalt, and a yellowish tuff. (Diorite is a granite-like igneous rock, but consists essentially of sodium-calcium feldspars with little or no quartz and potassium feldspar, while granite consists essentially of potassium feldspar and quartz.) The northern slope is covered with basaltic rock debris containing abundant inclusions of olivine, and other individual crystals, reaching five centimeters in length.

Mount Petras: From the air, the west side of Mount Petras appears to have the shape of a crater open to the north and occupied by a cirque glacier. Block-faulting apparently exists, with high-angle faults trending perpendicular to the mountain ridge, as indicated by zones of fault breccia and abundant striated, polished rock surfaces characteristic of fault planes.

Almost 25% of Mount Petras is exposed rock. The dominant rock type is a very fine-grained to coarse, granular rock, probably rhyolite, with large individual crystals in places. Pyrite is disseminated sparsely and randomly in a rhyolitic outcrop that is strikingly similar to the rhyolite found on the eastern mountain of the unnamed range (above).

Mountains and isolated peaks protrude

through the ice over a wide area. Pink granite intrudes a sequence of dark, well-stratified, partly metamorphased sedimentary rocks (metasediments). The granite contains large crystals of feldspar and ranges in texture from fine to very coarse grained. At Mount Van Valkenburg, the granite is intruded by two steep dikes of diorite; the "contact" area between the granite and the dike rock contains oval-shaped crystals of pink orthoclase feldspar and components of both granite and diorite.

At Mount Atwood, faults and joints in the granite are very conspicuous. A probable zone of faulting and brecciation, cleared of fine rock debris by very high winds, apparently created the split effect that gives the mountain two distinct peaks. The granite cliff walls contain well-rounded hollows, the result of wind abrasion with weathered granite crystals serving as the wind-carried abrasive.

The metasedimentary rocks overlying the granite are not greatly contorted by metamorphism, although some of the original sedimentary characteristics have been almost completely obliterated. The strata are intruded in many places by veinlets of quartz and fine-grained granite. Contact zones contain abundant mica, pyrite, and copper stains (malachite).

At Mount Van Valkenburg, the topography is controlled by the geologic structure. The saddle between the two peaks is in the plane of a high-angle, normal fault, which exhibits slickensides and brecciation.

Summary and Conclusions

Geological observations made thus far in West Antarctica indicate that the mountains visited (with the exception of the Clark Mountains) form an archipelago of isolated, volcanic "islands," trending generally east-west and possessing geologic and physiographic similarities. Further study of the rocks in this portion of Antarctica will help to determine its relationship to the remainder of Antarctica and to neighboring continents. Continued investigation is necessitated, moreover, by the failure thus far to observe major, broad-scale structural features in West Antarctica that can be correlated with features of neighboring and surrounding parts of the globe.

The NERV Experiment

The following report is based on material supplied by the National Aeronautics and Space Administration (NASA).

The NASA Nuclear Emulsion Recovery Vehicle (NERV) experiment was launched at 11:35 am EDT, September 19, 1960, from Point Arguello, California, as part of the United States contribution to the second International Rocket Interval (see *Bulletin No. 40*). The experiment was primarily designed to obtain detailed radiation measurements through part of the inner Van Allen belt of charged particles trapped in the Earth's magnetic field, and to return the information for study. NERV also carried a related biological experiment using mold spores.

The experimental vehicle, propelled by a newly designed Argo D-8 sounding rocket, reached an altitude of approximately 1200 miles and travelled 1200 miles downrange,

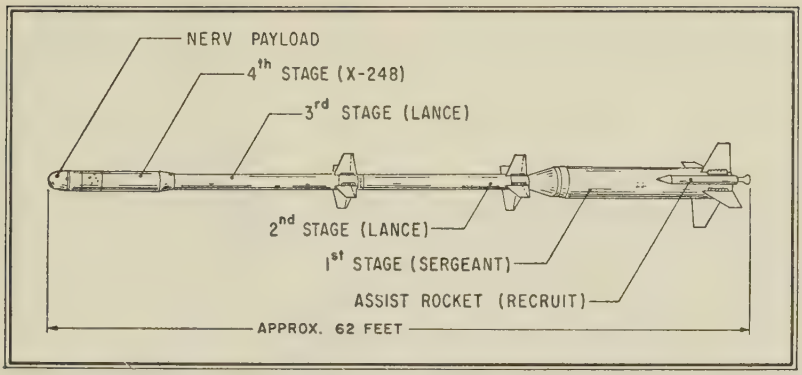

Fig. 8. *Argo D-8 Sounding Rocket Used in NERV Experiment.* (From NASA photograph.)

where it was recovered 2½ hours after launch by the *USS Rowan*, one of several US Navy vessels stationed in the impact area. This was the first flight of the Argo D-8 and, therefore, served also as a test of the new four-stage sounding rocket.

The NERV project is under the direction of NASA, with management responsibility assigned to NASA's Goddard Space Flight Center. Goddard conducted the emulsion experiment, and the mold-spore experiment was conducted by Florida State University. NERV was launched by the US Navy and was the first NASA rocket experiment flown from the West Coast. The Navy was also responsible for tracking and recovery operations.

Launch Vehicle

Aerolab Development Corporation (Pasadena, California), a subsidiary of the Ryan Aeronautical Company, manufactured the four-stage Argo D-8 launch vehicle (Fig. 8). The first stage, developed by the Thiokol Chemical Corporation, was a Sergeant rocket, which was assisted in the launch by two Recruit rockets attached to its sides. The second and third stages were Lance rockets developed by the Grand Central Rocket Company, and the fourth stage, an X-248 rocket, modified from the Vanguard final stage, was produced by the Allegany Ballistics Laboratories, a division of Hercules Powder Company.

Over-all length of the Argo D-8 was approximately 62 feet and its total weight was over 13,000 pounds. The unguided, solid-propellant launch vehicle gave the fourth stage a burnout velocity of more than 12,000 mph at an altitude of 124 miles, reached 95 seconds after liftoff. The fins of the first three stages were canted slightly, causing the stages to spin at 600 revolutions per minute during powered flight, thus providing spin stabilization for the fourth stage and payload.

NERV Payload

The complete NERV payload had an over-all length of 42 inches and a diameter of 19 inches. The payload was composed of two sections, the recovery vehicle and an adapter section that mated it to the fourth stage of the launch vehicle (see Fig. 9). The recovery vehicle was 16 inches long and was made of aluminum with an ablation heat shield. Including the experimental equipment, the vehicle weighed 83.6 pounds.

In addition to the experiments, NERV contained a programmer, two small electric motors, a battery supply, a parachute, and recovery aids such as radar chaff, a radio beacon, and a flashing light.

NERV was designed for aerodynamic stability during its re-entry into the atmosphere and drop into the sea. Just prior to re-entry, the payload was de-spun to 40 rpm by two weights attached to lines wound

around the adapter, and the nose cone was separated from the adapter. NERV then "righted itself" to a nose-first position to facilitate re-entry and opening of the parachute.

The cylindrical tungsten shield containing the nuclear emulsions was $\frac{5}{8}$ inch thick. In its side was a port approximately $\frac{2}{5}$ inch square (one centimeter) and covered by a layer of aluminum .004 inch thick. The aluminum seal kept the emulsions at sea-level pressure during the flight and prevented their exposure to sea water during recovery. The emulsion container section was $4\frac{3}{8}$ inches in diameter and, including a motor section (see below), $12\frac{1}{2}$ inches long. The emulsion stack was approximately $\frac{1}{2}$ inch long and 3 inches in diameter.

At an altitude of 300 statute miles on the upward leg of the NERV flight, the programmer activated a small electric motor which extended the shield $3\frac{1}{4}$ inches forward, exposing the emulsions to radiation (Fig. 9). They remained exposed through the crest of the trajectory and down to a height of 600 miles on the descent, where they were retracted for re-entry. Another motor rotated the emulsions while they were extended.

The three packages of neurospora for the biological experiment had a total weight of .18 pound. Pieces of foam weighing a total of 1.5 pounds were put into NERV to give it buoyancy in the water should seepage occur.

Approximately 10 seconds after the parachute opened, the flashing light and recovery beacon were activated. Both beacon and light had a planned lifetime of approximately 30 hours, to improve chances of recovery.

At water impact, about 37 minutes after liftoff, a block of fluorescein dye was released. A second block of dye was contained in water-soluble tape designed to deteriorate from interaction with sea water in about 4 hours, releasing more dye and thus giving the dye markers a total lifetime of approximately 12 hours. However, the vehicle was retrieved after only about $2\frac{1}{2}$ hours in the water.

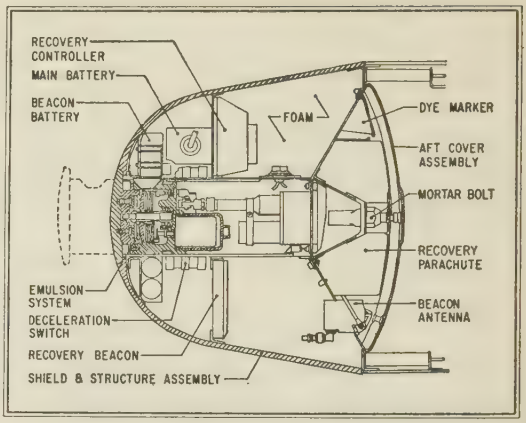

Fig. 9. *Cross section of NERV Payload. Dashed line at left indicates extended position of nuclear emulsion stacks. (From NASA photograph.)*

Emulsion Experiment

The NERV project is part of NASA's continuing program to investigate the nature, characteristics, history, and sources of the Van Allen radiation region. Studies based on data accumulated by the early Explorer satellites in 1958, conducted by James A. Van Allen and his colleagues at the State University of Iowa, revealed the presence of a region of high-intensity radiation trapped in the Earth's magnetic field. Subsequent studies, in particular those using the Pioneer space probes, provided further information about the extent, structure, composition, and temporal and spatial variations of the region (see *Bulletin No. 30*). Among other findings, these studies outlined within the vast region of geomagnetic trapping two belts—the "Van Allen belts"—in which the intensity of the trapped radiation is extremely high.

The data obtained in the NERV experiment will be of particular interest with regard to the interaction of the radiation region with the Earth's atmosphere and magnetic field. Since the NERV flight provided a profile of measurements through

part of the inner Van Allen belt, which begins at an altitude of 700 miles in this geomagnetic latitude, the results of the experiment will be used to help determine which of the various theories on the nature and characteristics of the inner region may best apply.

Results of the NERV experiment also pertain to future manned space flight. Since the radiation is continually changing and fluctuating in character, it is important to map the region in detail in order that adequate, minimum-weight shielding can be designed for manned flight through it. To do this, it is necessary to know the types of particles, their energy spectra, and the fluxes to be encountered.

The stack of 25 nuclear emulsions carried in the recovery vehicle were designed to record the passage of any charged particle with sufficient velocity to penetrate them—5 million electron volts (mev) or more. The particles leave "tracks" in the emulsions, thus producing a permanent record of the number of particles encountered as well as their charge, mass, velocity, and direction of travel in space relative to the emulsion.

The nuclear emulsions are similar to ordinary photographic emulsion, consisting of silver bromide grains embedded in a gelatin, but have a higher percentage of silver bromide and are much thicker. The nuclear emulsions used in the NERV experiment vary in sensitivity and thickness, but most are 600 microns thick (about 1/40 of an inch). Because of the thickness, almost two weeks were required to process these emulsions.

The shield around the emulsions prevented particles having energies of less than 150 mev from entering the emulsions except through the port. After the shield was extended forward, at the designated altitude, the stack was rotated behind the port, by a chronometrically driven motor, for one revolution during the period of exposure. The emulsions were nicked around their peripheries, and the nicks were aligned with the port and with a marked disk on top of the stack. When the stack was rotated, a time-sequence record of entering particles was thus obtained.

Measurement of the angular distribution of particles with respect to the lines of force of the Earth's magnetic field was achieved by the choice of an appropriate direction and angle of launch. The launch azimuth was 193° and the angle was 83° (or nearly vertical). During the rocket's ascent, its spin-axis paralleled the geomagnetic lines of force, making it possible to determine the angular distribution of particles in relation to the spin-axis. Thus, since the time, altitude, spin-rate, and attitude of the launch vehicle are known, a time history of the particles has been permanently recorded: i.e., the investigators can determine the number, distribution, velocity, angles, and directions of travel of the particles at a given position in the radiation region.

Biological Experiment

The three packages of neurospora (mold spores) carried inside the recovery vehicle were unprotected against radiation, and the intensities of radiation encountered were recorded by the emulsions. The spores are being studied for mutations resulting from their exposure to the known radiation field.

World Warning Agency Report
January 1 - June 30, 1960

The following report summarizes solar-terrestrial activity and related decisions of the World Warning Agency (AGIWARN) for the first half of 1960. Other reports in this series appear in earlier *Bulletins;* a review of geomagnetic disturbances and AGIWARN decisions for the IGC-1959 period was included in *Bulletin No. 39.*

The World Warning Agency, supported by the National Science Foundation and operated by the National Bureau of Standards at Fort Belvoir, Virginia, was established as part of the IGY World Days Program (see *Bulletin Nos. 2* and *5*). It continued to function on approximately the same level, with certain procedural modifications, during IGC-1959 (see *Bulletin No. 23*) and through June 1960. After June 30, 1960, when NSF support terminated, NBS assumed responsibility for much of the program.

AGIWARN Report: First Half, 1960

A total of 20 major solar flares (those classified 3 or 3+ in importance by at least one observatory) and 24 geomagnetic disturbances were recorded by AGIWARN during the period January 1-June 30, 1960. However, solar and geomagnetic activity were comparatively mild during the first quarter but became far more severe in the second three-month interval. A geomagnetic storm that began on March 31 was the most severe recorded since July 1959, and was associated with the longest radio disturbance in many years; in addition, the June 1 solar-flare was one of the largest observed in recent years.

First Quarter: AGIWARN recorded 10 geomagnetic disturbances during the first quarter of 1960, the quietest three-month interval from a geomagnetic and radio standpoint since before the IGY. The most significant disturbance was a geomagnetic storm that began on March 15 and reached maximum intensity early the next day, when a K-index of 6 was recorded (the K-index scale of magnetic disturbance ranges from 0, or very quiet, to 9, or extremely disturbed). This was the highest K-index of the year up to that time.

March 16 was also the only day of the quarter when the whole-day radio-quality index (weighted average of four 6-hour indices) was in the disturbed range. Of only seven disturbed 6-hour radio-quality indices during the quarter, five occurred during the March 15–17 storm.

The geomagnetic disturbances of January 5 and 13 began suddenly and are thought to have been associated with observed solar-flare activity. The other eight began gradually and were more typical of the kind of storms to be expected during this period of diminishing sunspot activity.

Second Quarter: During the April 1-June 30 interval, 10 out of a total of 12 geomagnetic disturbances were more severe than any that had occurred in the first three months of the year, and associated radio-propagation conditions were correspondingly much more disturbed. There was a total of 17 days for which the whole-day radio-quality index was in the disturbed range, and the number of 6-hour disturbed periods totaled 67 (March 31 is included in this count because the disturbance beginning on that date lasted through the first three days of April).

About half the geomagnetic disturbances in the second quarter appeared to be associated with solar events of relatively short duration and having well-defined, observable beginnings and endings. Included among these "event"-type disturbances,

however, were some geomagnetic storms that had gradual beginnings, while some storms that commenced suddenly could not be associated with observed solar activity at all. The major storms were all event associated.

The storm beginning on March 31, which was associated with an active solar region, was accompanied by severe and protracted disruption of high-frequency radio communications: for approximately 36 hours, radio quality was defined as useless. Although the storm that began on April 27, the quarter's second most severe disturbance, has not been linked with an observed solar event, sudden resurgences of geomagnetic activity on April 30 are believed to have been related to flare activity on the 28th. The third most important geomagnetic disturbance of the quarter, on May 8–9, was associated with observed flare activity.

A cosmic-ray-intensity increase on May 4 is thought to have been associated with the May 5 magnetic storm. This cosmic-ray increase is the only one for which Advance and World-wide Geophysical Alerts have been issued by AGIWARN (see *Bulletin No. 23*).

Solar and Geophysical Activity and AGIWARN Decisions, January 1-June 30, 1960: The following is a list of major solar flares, geomagnetic disturbances, World-wide Geophysical Alerts, and Special World Intervals (SWI) for the first half of 1960:

Jan	5	0202	Magnetic storm begins
	6	05xx*	Magnetic storm ends
	7	1504	Class 3 flare; S-SWF**
	10	06xx	Magnetic storm begins
	11	1600	Alert issued†
		2040	Class 3 flare; Slow S-SWF**
	12	03xx	Magnetic storm ends
	13	1900	Magnetic storm begins
	14	1600	Alert issued
	15	1352	Class 3 flare; Slow S-SWF
		18xx	Magnetic storm ends
	17	12xx	Magnetic storm begins
	18	1600	Alert issued
		21xx	Magnetic storm ends
	21	00xx	Magnetic storm begins
		1600	Alert issued
	25	00xx	Magnetic storm ends
Feb	5	06xx	Magnetic storm begins
		1600	Alert issued
			SWI starts††
	6	10xx	Magnetic storm ends
			SWI finishes
	13	19xx	Magnetic storm begins
	14	1600	Alert issued
		23xx	Magnetic storm ends
	16	09xx	Magnetic storm begins
		1600	Alert issued
	21	21xx	Magnetic storm ends
	22	1352	Class 3 flare; S-SWF
	26	0700	Class 3 flare
Mar	10	07xx	Magnetic storm begins
	11	22xx	Magnetic storm ends
	15	12xx	Magnetic storm begins
	16	1600	Alert issued
	17	22xx	Magnetic storm ends
	27	0657	Class 3 flare; Slow S-SWF
	29	0705	Class 3 flare; S-SWF
	31	08xx	Severe magnetic storm begins
		1600	Alert issued
			SWI starts
Apr	1	0854	Class 3 flare
		1600	Alert issued; auroras expected
	3	13xx	Severe magnetic storm ends
			SWI finishes
	5	0255	Class 3 flare; Slow S-SWF
	10	22xx	Magnetic storm begins
	12	0130	Class 3 flare
		1600	Alert issued
	13	12xx	Magnetic storm ends
	23	21xx	Magnetic storm begins
	24	1600	Alert issued
	26	11xx	Magnetic storm ends
	27	2000	Severe magnetic storms begins
	28	0130	Class 3 flare; Slow S-SWF
		1600	Alert issued; auroras expected
			SWI starts
	29	0209	Class 3 flare; Slow S-SWF
May	1	10xx	Severe magnetic storm ends
			SWI finishes
	4	1015	Class 3 flare; S-SWF
		1600	Alert issued for cosmic ray increase
	5	20xx	Magnetic storm begins
	6	1404	Class 3+ flare
	7	1600	Alert issued; auroras expected
			SWI starts
	8	00xx	Magnetic storm ends
		0422	Severe magnetic storm begins
		1600	Alert issued; auroras expected
	9	0704	Class 3+ flare
		11xx	Severe magnetic storm ends
			SWI finishes
	11	0438	Magnetic storm begins
		1600	Alert issued
	12	22xx	Magnetic storm ends
	13	0522	Class 3+ flare; S-SWF
	16	12xx	Magnetic storm begins
		1600	Alert issued
	17	14xx	Magnetic storm ends
	23	14xx	Magnetic storm begins
	24	1600	Alert issued
	25	05xx	Magnetic storm ends
	28	2020	Magnetic storm begins

	29	1600	Alert issued
	30	17xx	Magnetic storm ends
	31	16xx	Magnetic storm begins
June	1	0824	Class 3+ flare; Slow S-SWF
		15xx	Magnetic storm ends
	4	0250	Magnetic storm begins
		1600	Alert issued
			SWI starts
	6	18xx	Magnetic storm ends
			SWI finishes
	25	1136	Class 3 flare
		2040	Class 3 flare; S-SWF
	26	2358	Class 3 flare
	27	0145	Magnetic storm begins
		2140	Class 3 flare; Slow S-SWF
		1600	Alert issued
	29	08xx	Magnetic storm ends
		1937	Magnetic storm begins
	30	1600	Alert issued
Jul	2	17xx	Magnetic storm ends

* "xx" indicates gradual beginning or ending of a disturbance, following the hour indicated, such that the precise moment could not be determined.

** Symbols for ionospheric effects are defined as follows: S-SWF—sudden short-wave fadeout and gradual recovery; Slow S-SWF—slow short-wave fadeout (taking 5–15 minutes) and gradual recovery.

† No ending times for alerts are issued, as was done during the IGY; this is now left to the discretion of individual observatories.

†† SWI's, when warranted, start at the time the associated Alert is issued; they finish at the end of the day indicated.

IGY Bibliographic Notes

The following bibliographic references relating to IGY and IGC-1959 programs and findings were selected from a bibliography under preparation in the Science and Technology Division of the Library of Congress.

Yvette Avigon and Monique Pick-Gutmann: Relation entre les émissions solaires de rayons cosmiques et les sursauts de type IV. *Comptes rendus hebdomadaires des séances de l'académie des sciences.* (Paris). Vol. 249., no. 22. Nov. 30, 1959. Pp. 2276–2278. Diagr.

John C. Brandt and Joseph W. Chamberlain: Interplanetary Gas. I. Hydrogen Radiation in the Night Sky. *The Astrophysical Journal.* Vol. 130., no. 2. Sept. 1959. Pp. 670–682. Diagr.

M. W. Chiplonkar and P. V. Kulkarni: Contamination of the Intensities of the Oxygen Lines by the Neighboring OH Emission Bands in the Night Airglow. *Journal of Geophysical Research.* Vol. 64. no. 10. Oct. 1959. Pp. 1641–1642. Refs.

Committee on Space Research (COSPAR). Second Meeting, The Hague, March 12–14, 1959. *I. U. G. G. Chronicle.* No. 24. Nov. 1959. Pp. 292–300.

E. P. Fedorov: On the Publication and Reduction of the Latitude Observations Made During the International Geophysical Year. *Bulletin Géodésique* (Paris). No. 54. Dec. 1, 1959. Pp. 21–27.

Irène Fischer: The Hough Ellipsoid or the Figure of the Earth from Geoidal Heights. *Bulletin Géodésique* (Paris). No. 54, Dec. 1, 1959. Pp. 45–52. Diagr., map.

Samuel J. Goldstein, Jr.: The Angular Size of Short-Lived Solar Radio Disturbances. *The Astrophysical Journal.* Vol. 130, no. 2. Sept. 1959. Pp. 393–399. Diagr., illus.

E. E. Jesson: *Preliminary Report on Ice Thickness Measurements on the Antarctic Ice Cap by Seismic and Gravimetric Methods, 1958–1959.* Melbourne. 1959. 12 p. Map, 7 plates.

Atsushi Kimpara and Tatsuzo Obayashi: Geophysical Effects Associated with the High-Altitude Nuclear Explosion. Part II. Atmospherics. *Journal of Geomagnetism and Geoelectricity.* Vol. 11, no. 2. 1959. Pp. 48–50. Diagr. (Published also in *Comptes rendus hebdomadaires des séances de l'académie des sciences* (Paris). Vol. 248. Apr. 6, 1959; and *Nature.* Vol. 183. May 1959).

J. E. Lumby: The IGY World Data Centers for Oceanography. *Texas Journal of Science.* Sept. 1959. Pp. 259–269. Diagr., maps, refs.

Rolf Moore: A Rapid Method for Determination of Times and Paths over the Earth's Surface for Artificial Earth Satellites. *Astronautik* (Stockholm). Vol. 1, no. 2. 1958. Pp. 53–64. Illus., diagr.

J. F. Nye: Surface Topography of the Antarctic Ice Sheet. *Nature.* Vol. 184, no. 4689. Sept. 12, 1959. Pp. 786–787. Refs.

Publication of Microcards. *WMO Bulletin.* Vol. 8, no. 3. July 1959. Pp. 152–156. Illus.

Kuniji Saito, and Keizo Nishi: Attempts To Observe the Solar Ultraviolet Radiation with a Rocket-Borne Spectrograph. *Tokyo Astronomy Bulletin.* Second Series, no. 122. Nov. 20, 1959. Pp. 1497–1509. Illus., diagr.

Symposium On Antarctic Meteorology, Melbourne; 1959: *S. C. A. R. Bulletin.* No. 3, Sept. 1959, *in Polar Record,* Vol. 9, no. 63, Sept. 1959. Pp. 604–608.

Hiroyuki Uyeda and Saburo Ishikawa: Geophysical Effects Associated with the High-Altitude Nuclear Explosion. Part IV. Ionospheric Disturbances. *Journal of Geomagnetism and Geoelectricity.* Vol. 11, no. 2. 1959. Pp. 54–59. Diagr., map.

Preprinted from *Transactions, American Geophysical Union,* Vol. 41, No. 4, Dec. 1960